Adsorption 4, 149–158 (1998)

Effect of Operation Symmetry on Pressure Swing Adsorption Process

SHAIN J. DOONG AND PAUL PROPSNER
The BOC Group Technical Center, 100 Mountain Ave., Murray Hill, NJ 07974
shain.doong@us.gtc.boc.com

Abstract. In a multi-bed pressure swing adsorption (PSA) process, cycle steps with gas flow transferring from one bed to another such as equalization, purge, etc. are generally practiced to enhance the product recovery. However, if the flows for the connected beds in these steps are not balanced, the PSA process may not operate in a symmetrical manner. In the modeling of the PSA process, most of the simulations consider only one bed and assume that the rest of the beds would behave in a same way. In order to assess the impact of bed symmetry on the PSA performance, a new PSA model capable of studying bed symmetry in a two-bed system is developed. Experimental results from this paper show that uneven equalization flow can result in a lower product purity and a peculiar purity curve at different equalization levels. This phenomenon can be successfully predicted by this model. Simulation results also show that in large-scale PSA units, asymmetrical operation can cause drastically different temperature profiles in different adsorbers and hence a much lower performance. This paper demonstrates the importance of maintaining operation symmetry in PSA processes.

Keywords: pressure swing adsorption, gas separation, simulation

Introduction

Pressure swing adsorption (PSA) processes are widely used in industries for air and other gas separations. Most of these processes use multi adsorption columns to enhance product recovery as well as to maintain uninterrupted feed or product gas flow. For example, at least four beds are generally used for hydrogen PSA systems. And two or three beds are quite typical for nitrogen or oxygen PSA processes. More discussion about the applications and processes can be found in several monographs (Ruthven, 1984; Yang, 1987; Suzuki, 1990; Ruthven et al., 1994).

One characteristic of these multi-bed processes is that the gas exiting from one of the beds can be recycled back to the other bed. This can be seen in pressure equalization step, where the depressurizing gas of one bed is used to repressurize the other bed, or in purge step, where the effluent gas of one bed is used to regenerate the other bed. Actually, because of the number of possible configurations to send gas back and forth among the beds, numerous cycle sequences for the PSA processes have been developed. Obviously, the complexity of the PSA cycle also increases (Chiang, 1988). This presents a challenge to PSA process design and operation.

The other characteristic of the PSA process is that each bed is undergoing the same step sequence in a cyclic way. But at any one time, each bed is performing different functions at a different step of the cycle. Ideally, the separation performance of each bed is expected to be the same. To this end, a PSA plant would require a symmetrical setup for the plant pipings, valvings, adsorbent packing, etc. From an operational point of view, gas flows, pressures, and temperatures all need to be balanced in each bed and during every cycle. Due to the dynamic nature of the PSA process, these variables tend to be very difficult to control or measure. Any disturbance in the system, such as ambient temperature, ambient pressure, switching valve positions, etc., could tip the balance and result in an asymmetrical operation for a PSA plant. As a consequence, each PSA bed may no longer operate at the same pressure swing or processing the same amount of gas. The impact of

operation symmetry on the PSA process performance is currently unanswered.

Concurrent with the wide commercialization of the PSA processes are the increasing research efforts focused on the theoretical simulation of these processes. Simulation of PSA processes requires solving complex partial differential equations related to the mass and energy balances in the adsorption column. These equations are then solved by numerical techniques, which can be quite time consuming. To alleviate this computational burden, most of the PSA models take advantage of the cyclic nature of the PSA processes and assume that each bed is behaving the same way (Doong and Yang, 1987; Kumar et al., 1994). Consequently, a solution of only one adsorber needs to be obtained. The drawback of this type of model is its inability to describe the real dynamics of the entire PSA plant. Furthermore, it is not capable of addressing the symmetry issue for the PSA processes.

In this paper, the effect of operational symmetry on PSA process performance is examined by both experiments and simulations. A new PSA model capable of studying bed symmetry in a two-bed system is developed. The simulation results are compared with experimental data to demonstrate the effect of asymmetrical purge and bed equalization for a PSA oxygen system.

Process Description

A two-bed Skarstrom's cycle (Skarstrom, 1972) with bed to bed equalization steps is used as an example for the symmetry study. The cycle steps are described below.

1. Adsorption step: Feed gas passes from one end of the bed and product gas is produced from the other end.
2. Equalization step: Feed is terminated and the bed is depressurized by transferring gas to the other bed through the product end.
3. Vent step: The bed is further depressurized through the feed end.
4. Purge step: The bed is regenerated with a portion of the product gas from the other bed, which is generated in step 1.
5. Bed equalization step: The bed is repressurized from the product end using the depressurization gas from the other bed undergoing step 2.
6. Feed pressurization step: The bed is pressurized by the feed gas.

Modeling of PSA process with Asymmetrical Flows

A PSA process simulator developed previously (LaCava et al., 1989) was modified to address the symmetry issue in this study. This simulator contains a rigorous mathematical model describing the transport phenomena in adsorption columns, which involves mass balance, energy balance, adsorption equilibrium, mass transfer, heat transfer, etc. For the case of asymmetrical flow, the fundamental assumptions and equations remain the same. They are described briefly below.

The assumptions made in the derivation of the model are ideal gas law, no axial pressure gradient across the bed, thermal equilibrium between the fluid and solid phases, and no variation exists in the radial direction for both concentration and temperature.

Mass balances for the gas species in a packed bed are:

$$\varepsilon\frac{\partial C_i}{\partial t}+\frac{\partial uC_i}{\partial z}-D_L\frac{\partial^2 C_i}{\partial z^2}-s_i=0 \quad i=1,\ldots,n \tag{1}$$

where ε is the interparticle void fraction, C_i is the concentration of component i in the gas phase, u is the superficial velocity, z is the bed distance, D_L is the axial dispersion coefficient, and s_i is the sorption rate per unit volume of the bed for component i.

It is convenient to express the above equations in dimensionless form for the purpose of numerical solutions. Thus, summing Eq. (1) for all the components, and applying the ideal gas law, one can obtain the following dimensionless equations:

$$\varepsilon\frac{\partial Y_i}{\partial \tau}+U\frac{\partial Y_i}{\partial Z}+Y_i\frac{\bar{T}}{\bar{P}}\sum_{j=1}^{n}S_j-\frac{\bar{T}}{\bar{P}}S_i-\frac{1}{\mathrm{Pe}_L}\frac{\partial^2 Y_i}{\partial Z^2}=0 \tag{2}$$

$$\varepsilon\frac{1}{\bar{P}}\frac{\partial \bar{P}}{\partial \tau}+\frac{\partial U}{\partial Z}-\frac{U}{\bar{T}}\frac{\partial \bar{T}}{\partial Z}-\frac{\varepsilon}{\bar{T}}\frac{\partial \bar{T}}{\partial \tau}-\frac{\bar{T}}{\bar{P}}\sum_{j=1}^{n}S_j+\frac{1}{\mathrm{Pe}_L}\frac{\partial^2 \bar{T}}{\partial Z^2}-\frac{2}{\mathrm{Pe}_L\bar{T}^2}\left(\frac{\partial \bar{T}}{\partial Z}\right)=0 \tag{3}$$

where

$$\bar{T} = T/T_0, \quad \bar{P} = P/P_0, \quad Z = z/L, \quad \tau = tu_0/L,$$
$$U = u/u_0, \quad \mathrm{Pe}_L = u_0 L/D_L,$$
$$S_j = (s_j)/(u_0/L)/P_0/(RT_0)$$

Y_i is the mole fraction of component i in the gas phase, L is the bed length, T is temperature and P is pressure.

Energy balance in the bed gives:

$$\frac{\partial}{\partial t}\left\{\left(\varepsilon C_{pg}C + \rho_B C_{ps} + \rho_B C_{pg}\sum_{j=1}^{n} q_j\right)T\right\} + \frac{\partial(uC_{pg}CT)}{\partial z} - K_L\frac{\partial^2 T}{\partial^2 z} - \sum_{j=1}^{n}\Delta H_j\frac{\partial q_j}{\partial t}\rho_B + \frac{4h_w}{d_i}(T - T_w) = 0 \tag{4}$$

where C_{pg} is the heat capacity of the gas, C is the overall gas concentration in the gas phase, ρ_B is the bulk density of the adsorbent, C_{ps} is the heat capacity of the adsorbent, q_j is the adsorption amount in the solid phase for component j, ΔH_j is the heat of adsorption, h_w is the heat transfer coefficient between the packed bed and the wall, K_L is the axial thermal conductivity, and d_i is the inside diameter of the bed, T_w is the average wall temperature.

Another energy balance equation can be written for the wall of the bed:

$$A_w\rho_w C_{pw}\frac{\partial T_w}{\partial t} = \pi d_i h_w(T - T_w) - \pi d_o h_0(T_w - T_a) + K_w A_w\frac{\partial^2 T_w}{\partial z^2} \tag{5}$$

where A_w is the cross section area of the wall, ρ_w is the density of the wall, C_{pw} is the heat capacity of the wall, d_o is the outside diameter of the bed, K_w is the thermal conductivity of the wall, T_a is ambient temperature, h_0 is the heat transfer coefficient between the wall and ambient.

Combining Eqs. (3) and (4) and neglecting the terms containing D_L, one obtains the following dimensionless energy equation:

$$\frac{\partial\bar{T}}{\partial\tau} + \delta_1 U\frac{\partial\bar{T}}{\partial Z} - \frac{1}{\mathrm{Pe}_h}\frac{\partial^2\bar{T}}{\partial Z^2} - \sum_{j=1}^{n}\delta_{2j}\frac{\partial Q_i}{\partial\tau} + \delta_3(\bar{T} - \bar{T}_w) = 0 \tag{6}$$

Equation (5) becomes:

$$\frac{\partial\bar{T}_w}{\partial\tau} = \beta_1\bar{T} + \beta_2\frac{\partial^2\bar{T}_w}{\partial Z^2} - \beta_3\bar{T} + \beta_4\bar{T}_0 \tag{7}$$

where

$$Q_j = \frac{q_j}{q_{jo}},$$
$$\delta_1 = C_{pg}C\Big/\left(\varepsilon C_{pg}C + \rho_B C_{ps} + \rho_B C_{pg}\sum_j q_j\right),$$
$$\delta_{2j} = \rho_B q_{jo}\Delta H_j\Big/\left(\varepsilon C_{pg}C + \rho_B C_{ps} + \rho_B C_{pg}\sum_j q_j\right),$$
$$\mathrm{Pe}_h = u_0 L\left(\varepsilon C_{pg}C + \rho_B C_{ps} + \rho_B C_{pg}\sum_j q_j\right)\Big/K_L,$$
$$\delta_3 = 4h_w L/u_0 d_i\Big/\left(\varepsilon C_{pg}C + \rho_B C_{ps} + \rho_B C_{pg}\sum_j q_j\right),$$
$$\beta_1 = \pi d_i h_w L/(A_w\rho_w C_{pw}u_0),$$
$$\beta_2 = K_w A_w/(A_w\rho_w C_{pw}u_0 L),$$
$$\beta_3 = \pi(d_i h_w + d_o h_0)L/(A_w\rho_w C_{pw}u_0),$$
$$\beta_4 = \pi d_o h_0 L/(A_w\rho_w C_{pw}u_0)$$

In this paper, the familiar linear driving force (LDF) model is used to describe the mass transfer resistance. The sorption rate is expressed by:

$$S_i = -\rho_B\frac{q_{io}RT_0}{P_0}\frac{\partial Q_i}{\partial\tau} = -\rho_B k\frac{L}{u_0}\frac{q_{io}RT_0}{P_0}\left(Q_i^s - Q_i\right) \tag{8}$$

where k is the linear rate coefficient, Q_i^s is the equilibrium adsorption amount at gas phase composition Y_i.

Method of Solution

Equations (2), (3), (6), and (7) constitute a set of nonlinear partial differential equations, coupled with the rate equation, Eq. (8). A finite difference method is employed to convert them into ordinary differential equations. Standard time integrators such as Runge Kutta or Gear method is then used to solve them. Boundary and initial conditions can be written based on the steps of the PSA process. Although the direction of the gas flow in a PSA bed can switch depending on the step sequence, the condition at one end of the bed is always known. For example, the flow is zero at one end

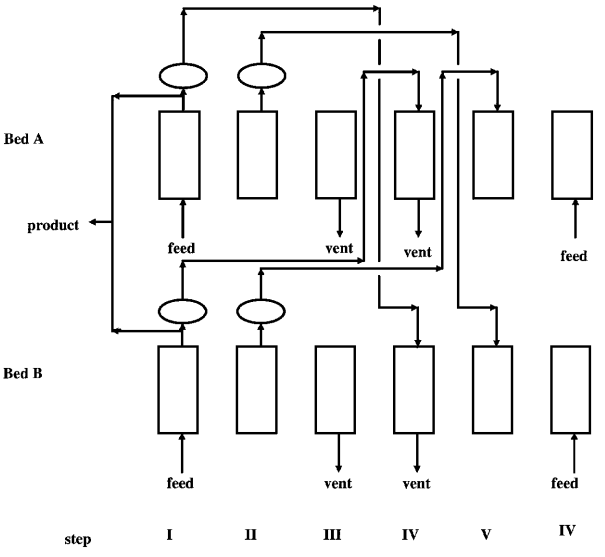

Figure 1. Flow diagram of PSA process simulator for a 2-bed 6-step cycle.

of the bed during pressurization, equalization or vent step. Thus the gas flow at the other end of the bed can be calculated. The pressure profile is known input parameter in this model.

To simulate the previously described two-bed six-step cycle, the effluents from one bed are temporarily stored and then used as inlet streams for the other bed in the next cycle. Figure 1 is a flow diagram illustrating this concept. Part of the product produced from bed A is stored and then used as the purge stream for bed B in the next cycle. This determines the boundary condition for the purge step. Similarly, the depressurization gas from bed A during the equalization step is also stored and used as the pressurization gas for bed B in the following cycle. In this case, as the flow conditions at both ends of the bed are known, the end pressure of the equalization step for bed B is calculated by the model, not specified by the user. Instead of solving the equations for both beds simultaneously, the solution for each bed is calculated alternately between the cycles. To simulate asymmetrical flows, the streams used for the purge or equalization step can be arbitrarily set to be different for each bed. However, the mass balance still needs to be satisfied so that the same amount of equalization gas or purge gas supplied from one bed is used for the other bed. The final product purity is taken as an average from both beds. The traditional way to solve a multibed system is to assume that purge or equalization flows between the two beds are identical. Therefore, the effluent streams are used for the same bed during a later process step of the same cycle (Doong and Yang, 1987; Kumar et al., 1994).

Obviously the simplified model proposed in this paper is still unable to predict the real dynamics of a multibed system. It is, however, capable of examining the impact of process symmetry on its performance. For example, in addition to the asymmetrical purge or equalization flow, one can also study the effect of uneven feed flows or unequal adsorbent packing among beds.

Experimentals

A two-bed apparatus, as shown in Fig. 2, was set up for this study. The system consisted of two adsorption columns, each 85 cm long and 6.7 cm I.D. The columns were packed with 760 gm of UOP 5AMG zeolite. Mass flow meters by Brooks were used to measure air feed, oxygen product, purge and equalization flow rates. Oxygen purity was measured by a Servomax oxygen analyzer. Two pressure transducers were located at the top of the beds. Switching valves were of the solenoid type. A Mitsubishi PLC (programming logic controller), F2-6M was used to control the cycle sequence.

Experiments were performed at a feed pressure of 3.3 atm and a regeneration pressure of 1 atm. The half cycle time was 45 sec, with 14 sec pressurization/vent, 25 sec production/purge and 6 sec equalization. For symmetrical equalization operation, valves 6 and 7

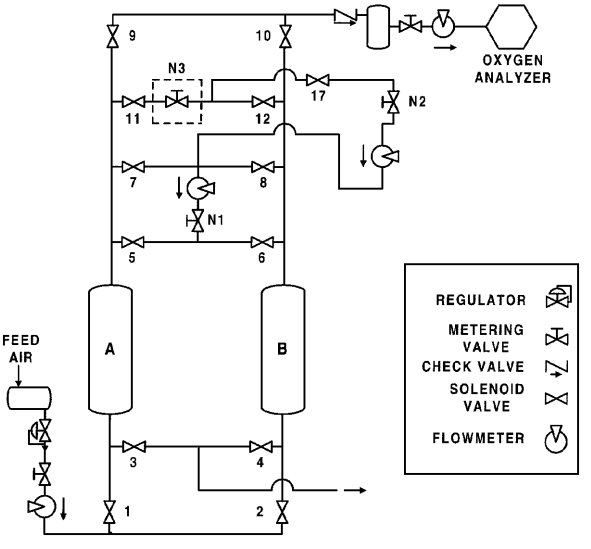

Figure 2. Experimental apparatus.

were open for one direction of equalization flow and valves 5 and 8 were open for the other direction. Manual needle valve N1 was then used to adjust the equalization flows. For asymmetrical equalization flow, valves 6 and 7 were open for both directions of flow. Different equalization flows were obtained since a needle valve has different flow characteristics when the flow direction is reversed.

To implement the purge step, valves 11, 17 and 8 were opened to purge from bed A to B, and valves 12, 17 and 7 were opened to purge from B to A. Manual valve N2 was used to adjust the purge flow rates. For asymmetrical purge flows, additional needle valve N3 was installed to reduce the purge flow from bed A to B. PSA performance was measured by the product flow and product yield. The later is defined as the amount of oxygen in the product divided by the amount of oxygen in the feed. Normally, it took about 2 hours to reach a steady state from start-up.

Results and Discussion

Effect of Asymmetrical Flow in Equalization Step

The experimental results for the product purity at different equalization levels are shown in Fig. 3, for the same product flow rate. The equalization level is represented by the final pressure of the one bed that is receiving the equalization gas or the pressure-rising bed. For the case of symmetrical equalization flow, there appears an optimal equalization level for the maximum product purity. In the case of asymmetrical equalization flow, the

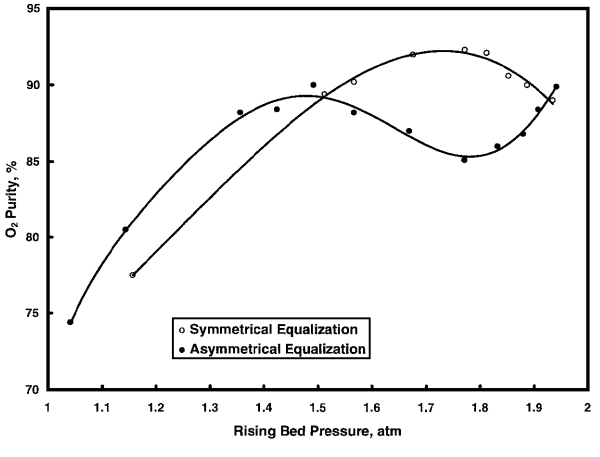

Figure 3. Effect of asymmetrical equalization on product purity from experimental results. (Curves drawn to smooth out data.)

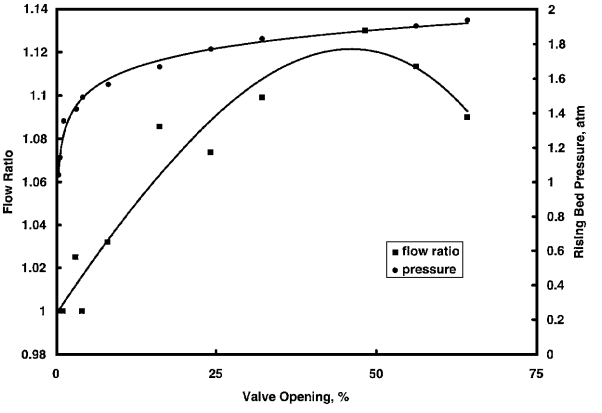

Figure 4. Measured flow ratios (forward flow/backward flow) and equalization pressures at different valve openings for a needle valve. (Curves drawn to smooth out data.)

purity first increases with increasing level of equalization, then starts to decline at a pressure about 1.5 atm and finally increases again at a pressure about 1.8 atm. This peculiar functionality of product purity vs. equalization level is primarily due to the characteristics of the needle valve used in the experiment. The needle valve gives a maximum uneven flow at about 40% opening, as shown in Fig. 4, where the ratio of forward flow vs. backward flow is plotted against valve opening. Also shown in Fig. 4 are the equalization pressures for the pressure-rising bed corresponding to the valve openings used in the experiment. The difference of equalization flows between the two beds can be up to 13%, where the equalization pressure is about 1.8 atm. This is also the pressure where the purity reaches a minimum for the asymmetrical case in Fig. 3.

One might expect different equalization pressures for each bed when the equalization flows are not the same. The pressure actually is insensitive to the difference of equalization flows. Figure 5 shows the pressure profile of both beds for the case where the equalization flow difference is about 13%. It is difficult to observe any symmetry problem from the pressure profile alone. The product purity, however, drops from 92% for the symmetrical case to 85%, as seen in Fig. 3.

Verification of Model

Before the model was used to study the symmetry effect, it was first verified with experimental data for a cycle with symmetrical flows in both purge and equalization steps. This was done by adjusting the kinetic constant of the linear driving force expression

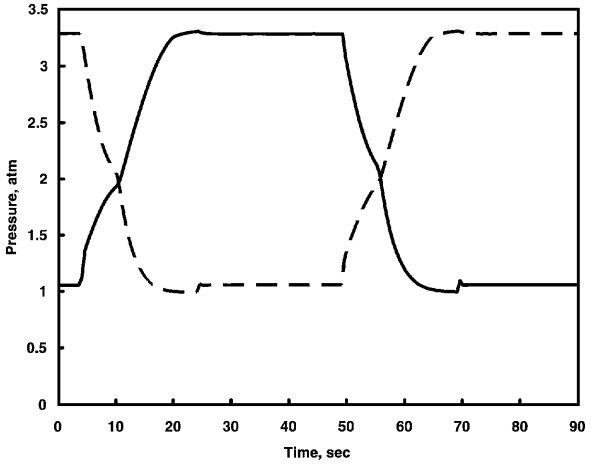

Figure 5. Bed pressure profiles with asymmetrical equalization flows from experimental data.

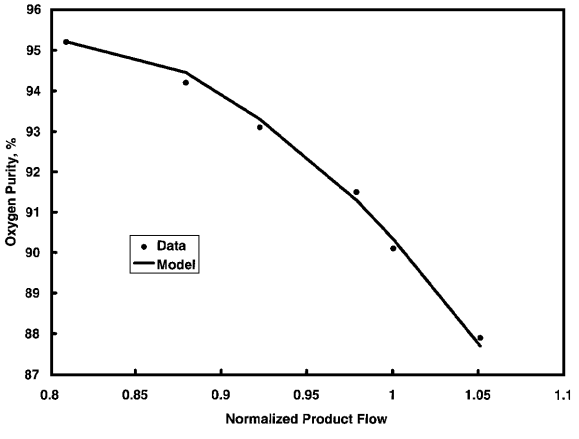

Figure 6. Comparison of experimental data and simulation results for oxygen purities at different product flows.

in the model until the simulation results fit the data for a range of purities. The kinetics in a PSA system can be characterized by the purity curves generated by running different product flows, in a way similar to the adsorption breakthrough curve. Consequently, fitting a range of purities, instead of a single point, can better represent the system kinetics. Figures 6 and 7 show the comparison between the model and experimental data for the product flow and the product yield, respectively. The pressure at the end of equalization was 1.7 atm for the pressure-rising bed. The kinetic constant was 2.1 1/sec. In the simulation, the adsorption isotherms and other related physical properties for this 5A zeolite were taken from Miller et al. (1987). A summary of parameters used in the simulation is listed in Table 1.

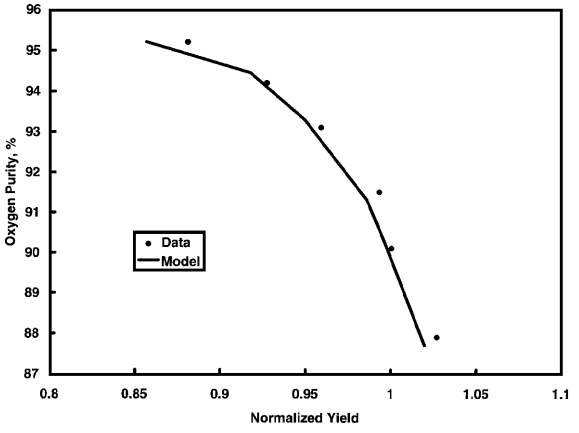

Figure 7. Comparison of experimental data and simulation results for oxygen purities at different product yields.

The initial conditions of the bed can be either a clean bed saturated with 100% oxygen or any concentration profile from previous simulation results. Therefore, the bed profile obtained from the symmetrical operation can be used as an initial condition for the case of asymmetrical operation by simply varying the equalization flows or purge flows between the two beds. The steady state solution of the simulation is found to be independent of the initial conditions. Steady state solution can be achieved in about 100 cycles for a small PSA unit. However, at least 1000 cycles are needed for a large-scale unit to achieve steady state. No stability problem has been encountered in this simulator.

Simulation Results

The model with the fitted kinetic constant was then applied to the cases with different equalization flows between the two beds. The result is shown in Fig. 8 for different ratios of equalization flows at various levels of equalization pressures. As expected, large equalization flow ratios, i.e., more asymmetrical equalization, yield lower product purities. Obviously, the effect of symmetry becomes diminished at low levels of equalization because the contribution of the equalization step to the process performance becomes insignificant.

Figure 8 also shows that the maximum purity occurs at a pressure about 1.4 atm for the symmetrical case, whereas the experimental data gives a pressure about 1.8 atm as shown in Fig. 3. The reason for this discrepancy is still not clear. The assumption of no pressure drop in the simulation, especially during the equalization step, could be one contributing factor.

Table 1. Values of parameters used in the simulation.

Saturation capacity, V_m (mole/gm)	4.13×10^{-3}
Equilibrium constant for N_2, B_1 (1/atm)	$2.2 \times 10^{-4} \exp(1898/T)$
Equilibrium constant for O_2, B_2(1/atm)	$1.54 \times 10^{-4} \exp(1622/T)$
Constant in Langmuir-Sips equation for N_2, n_1	1.424–178.5/T
Constant in Langmuir-Sips equation for O_2, n_2	1
Heat of adsorption for N_2, ΔH_j (J/mol)	25080
Heat of adsorption for O_2, ΔH_j (J/mol)	12540
Void fraction, ε	0.52
Bed bulk density, ρ_B (g/cc)	0.79
Heat capacity of the adsorbent, C_{ps}, (J/gm/K)	0.92
Heat capacity of the wall, C_{pw} (J/gm/K)	0.46
Density of the wall, ρ_w (gm/cm^3)	7.8
Axial thermal conductivity, K_L (J/cm/sec/K)	4.18×10^{-3}
Thermal conductivity of the wall, K_w (J/cm/sec/K)	0.45
Heat transfer coefficient between the wall and ambient, h_0 (J/cm^2/sec/K)	4.18×10^{-3}
Heat transfer coefficient between the packing and the wall, h_w (J/cm^2/sec/K)	4.18×10^{-3}

Langmuir-Sips equation $q_i = \frac{V_m B_i P_i^{n_i}}{1+\sum B_i P_i^{n_i}}$.

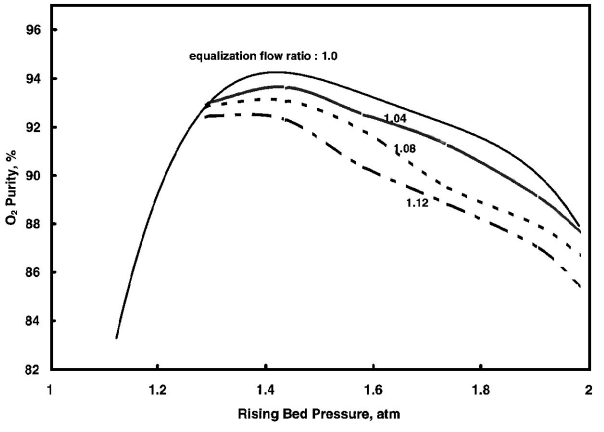

Figure 8. Effect of asymmetrical equalization on product purity from simulation results at various equalization flow ratios between the two beds.

Additionally, the system may be far away from equilibrium conditions during the fast equalization step, which has only 6 sec. The use of the LDF approximation may break down under this circumstance (Nakao and Suzuki, 1983).

Effect of Asymmetrical Purge

The purge step can also create a symmetry problem in a PSA process, especially when the purge gas is directly provided from one bed to the other. To examine this effect, the purge flow to one bed was first adjusted to be about 3% higher than the other bed. Next, the difference of this unequal purge flow was set to 13%. The average purge flows for both beds, however, were kept the same. The performances relative to the case with symmetrical purge flow are shown in Table 2 for both experiment and simulation. It can be inferred from this table that PSA performance may decline if there is more than 10% difference between the purge flows of the two beds. The model also successfully predicts the trend of the asymmetrical purge effect on purity.

Table 2. Effect of purge asymmetry on PSA performance.

Purge ratio	Experiment		Simulation	
	Relative yield	O_2 purity	Relative yield	O_2 purity
1	1.0	91.1	1.0	91.3
1.03	0.99	90.3	0.99	90.0
1.13	0.94	85.1	0.91	80.6

When a PSA process is operating in an asymmetrical way, one of the beds may produce higher purity than the other. Consequently, there will be a mixing of different product purities, which tends to drop the separation efficiency. For example, with a purge ratio between the two beds of 1.13 as in Table 2, one bed produces 87.8% oxygen purity product while the other bed is

73.4% purity. The overall product purity is 80.6%. Not only is the net product purity lower than the case of symmetrical purge flow, but both beds also generate lower purity individually. Over-purge of one PSA bed can not compensate for the loss of performance from under-purge of the other bed.

Effect on Large-Scale Unit

The other important variable that can also be affected by the symmetry of a PSA process is bed temperature. As is known, significant axial temperature gradients can only be generated in relatively large-scale PSA systems and not in small bench units (Collins, 1976). As energy balance equations are included in the model developed in this paper, it can be easily applied to examine the symmetry impact on bed temperature.

The same conditions used for the above bench study are applied to a large-scale unit with a bed diameter of 1 meter and a bed length of 1.7 meter. With a 10% difference in purge flow between the two beds, the simulation predicts a product purity of 74.4%, as compared to 88% for a symmetrical purge flow. The bed temperature profiles generated from the simulation for the case of asymmetrical purge flow are plotted in Fig. 9 for both beds. As can be seen, the temperature profiles of each bed are quite different. The bed that is receiving higher purge shows a colder temperature at the bottom of the bed than the one that is receiving lower purge. With asymmetrical purge flows, the performance of a PSA plant can be significantly decreased by drastically different bed temperatures (Schaub et al., 1995). Different bed temperatures, which result in different adsorption capacities for the sieve, may induce different flow patterns and cause further asymmetry problem.

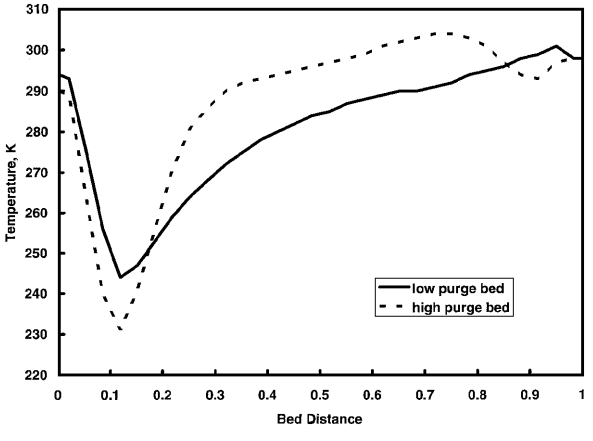

Figure 9. Effect of asymmetrical purge on bed temperature for a large-scale PSA unit from simulation results.

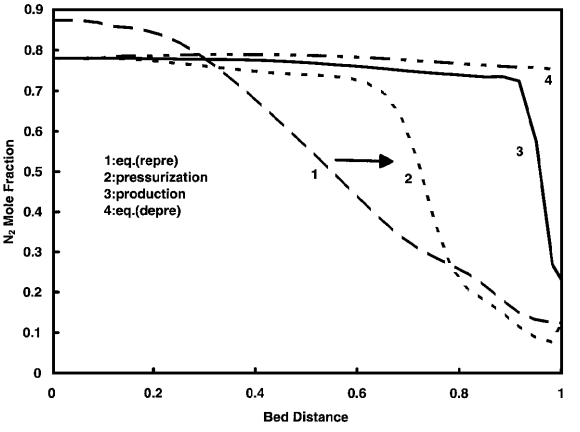

Figure 10. Bed concentration profiles at the end of PSA step for the bed that receives less purge from simulation results.

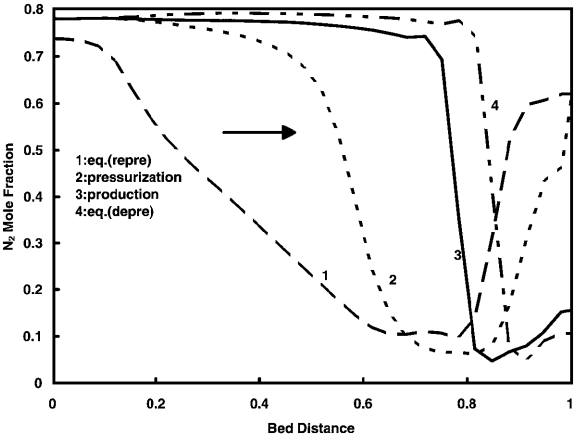

Figure 11. Bed concentration profiles at the end of PSA step for the bed that receives more purge from simulation results.

To further understand the effect of asymmetrical purge on the PSA performance, the bed concentration profiles generated from the simulation for the above large-scale unit are plotted in Figs. 10 and 11 for each bed. Only the profiles at the end of equalization step with pressure rising, feed pressurization step, adsorption step and equalization step with pressure decreasing are shown in the figures. Figure 10 is the concentration profile for the bed that is receiving less purge gas. The nitrogen concentration wave front appears to breakthrough at the end of the production step. At the end of the equalization step (depressurization), the effluent contains up to 78% of nitrogen. This poor quality gas is used to repressurize the other

bed during the equalization step (repressurization), as shown in Fig. 11 for the bed that is receiving more purge gas. The product end of this bed is contaminated, giving rise to a low purity of product gas. The main nitrogen wave front is still not reaching breakthrough after the production and equalization steps, probably due to better regeneration by the use of high purge. In spite of that, the high purge bed actually produces lower purity than the low purge bed. One can expect even more complex dynamics if the equalization flows are additionally asymmetrical. The simulation offers a very useful tool to diagnose symmetry problems that may be encountered in actual plants.

Conclusions

A PSA process simulator was developed to analyze the effect of operation symmetry on PSA performance. The simulation successfully predicts the effect of asymmetrical flows in the purge and equalization steps for a two-bed PSA oxygen system. Both simulation and experimental results show that a significant drop in the product purity can occur when there is more than 10% difference of flows between the two beds in either the purge or equalization step. In large-scale PSA units, the simulation also shows that asymmetrical operation can cause drastically different temperature profiles in different adsorbers. The simulation offers a very useful tool to diagnose the potential problems that may be encountered in actual plants.

Nomenclature

A_w	Cross section area of the wall	cm^2
C	Gas phase concentration	mole/cc
C_{pg}	Heat capacity of the gas	J/mol/K
C_{ps}	Heat capacity of the adsorbent	J/gm/K
C_{pw}	Heat capacity of the wall	J/gm/K
d_i	Inside diameter of the bed	cm
d_o	Outside diameter of the bed	cm
D_L	Axial dispersion coefficient	cm^2/sec
h_0	Heat transfer coefficient between the wall and ambient	J/cm^2/sec/K
h_w	Heat transfer coefficient between the packed bed and the wall	J/cm^2/sec/K
K_L	Axial thermal conductivity	J/cm/sec/K
K_w	Thermal conductivity of the wall	J/cm/sec/K
k	Linear driving force coefficient	1/sec
L	Bed length	cm
P	Pressure	atm
Pe_L	Peclet number for mass transfer	—
Pe_h	Peclet number for heat transfer	—
Q_i^s	Dimensionless equilibrium adsorption amount at gas phase composition Y_i	—
q	Adsorption amount in the solid phase	mol/gm
R	Gas constant	—
S_i	Dimensionless sorption rate	—
s_i	Sorption rate per unit volume of the bed for component i	mol/cm^3/sec
T	Bed temperature	K
T_a	Ambient temperature	K
T_w	Average wall temperature	K
t	Time	sec
U	Dimensionless superficial velocity	—
u	Superficial velocity	cm/sec
Z	Dimensionless bed distance	—
z	Bed distance	cm

Greek Letters

ε	Interparticle void fraction	—
ρ_B	Bulk density of the adsorbent	gm/mol
ρ_w	Density of the wall	gm/cm^3
ΔH_j	Heat of adsorption for component j	J/mol
τ	Dimensionless time	—

Subscripts

i	Gas component
o	Characteristic quantity

References

Chiang, A.S.T., "Arithmetic of PSA Process Scheduling," *AIChE J.*, **11**, 1910–1912 (1988).

Collins, J.J., "Air Separation by Adsorption," US Patent 3,973,931 (1976).

Doong, S.J. and R.T. Yang, "Hydrogen Purification by the Multibed Pressure Swing Adsorption Process," *Reactive Polymers*, **6**, 7–13 (1987).

Kumar, R., V.G. Fox, D.G. Hartzog, R.E. Larson, Y.C. Chen, P.A. Houghton, and T. Naheiri, "A Versatile Process Simulator for Adsorptive Separation," *Chem. Engr. Sci.*, **49**(18), 3115–3125 (1994).

LaCava, A.I., J.A. Dominguez, and J. Cardenas, "Modeling and Simulation of Rate Induced PSA Separations," *Adsorption: Science*

and Technology, A.E. Rodrigues, M.D. LeVan, and D. Tondeur (Eds.), NATO ASI Series, vol. 158, pp. 323–337, 1989.

Miller, G.W., K.S. Knaebel, and K.G. Ikels, "Equilibrium of Nitrogen, Oxygen, Argon, and Air in Molecular Sieve 5A," *AIChE J.*, **33**, 194–201 (1987).

Nakao, S. and M. Suzuki, "Mass Transfer Coefficient in Cyclic Adsorption and Desorption," *J. Chem. Eng. Japan*, **15**, 114 (1983).

Ruthven, D.M., *Principles of Adsorption and Adsorption Processes*, Wiley, New York, 1984.

Ruthven, D.M., S. Farooq, and K.S. Knaebel, *Pressure Swing Adsorption*, VCH Publishers, New York, 1994.

Schaub, H.R., J. Smolarek, F.W. Leavitt, L.J. Toussaint, and K.A. LaSala, "Tuning of Vacuum Pressure Swing Adsorption Systems," US Patent 5,407,465 (1995).

Skarstrom, C.W., "Heatless Fractionation of Gases Over Solid Adsorbents," *Recent Development in Separation Science*, N.N. Li (Ed.), vol. 2, CRC Press, 1972.

Suzuki, M., *Adsorption Engineering*, Chemical Engineering Monographs 25, Tokyo and Elsevier Science Publishers, Kodansha, 1990.

Yang, R.T., *Gas Separation by Adsorption Processes*, Butterworths, Boston, 1987.